Effect of Shock Heating on the Stability of Laser-Driven Targets

T. R. Boehly,[1] J. A. Delettrez,[1] J. P. Knauer,[1] D. D. Meyerhofer,[1] B. Yaakobi,[1] R. P. J. Town,[1] and D. Hoarty[2]

[1]*Laboratory for Laser Energetics, Department of Physics and Astronomy, and Department of Mechanical Engineering, University of Rochester, 250 East River Road, Rochester, New York 14623-1299*

[2]*Atomic Weapons Establishment, Aldermaston, Reading RG7 4PR, United Kingdom*

(Received 30 November 2000; published 17 September 2001)

The shock heating of a laser-driven, direct-drive target can determine its stability by affecting Rayleigh-Taylor growth rates through target decompression and ablative stabilization. Measurements indicate that pulses that rise rapidly to 10^{14} W/cm^2 produce shock-induced temperatures of ~25 eV, whereas more slowly rising pulses show less heating. Analysis of the observed target behavior produced by these two pulses demonstrates that shock heating improves hydrodynamic stability because ablative stabilization increases when the targets are preheated by shocks.

DOI: 10.1103/PhysRevLett.87.145003 PACS numbers: 52.50.Lp, 52.35.Py, 52.35.Tc

Hydrodynamic instability is a key issue for inertial confinement fusion (ICF) [1–3]. The effects of the Rayleigh-Taylor (RT) instability can be reduced by shocks that heat the target shell, causing a slight decompression; this increases the ablation velocity and reduces the RT growth rate [4–6]. ICF target designs use shock heating to determine the implosion isentrope and establish a balance between performance and stability. Direct-drive experiments planned for the National Ignition Facility [7] are expected to produce implosions [2] that have $\alpha = 3$ isentropes. The heating that increases the isentrope provides a reduction in RT growth and only moderately reduces the gain of the target. To validate the codes used to produce these designs, it is important that the shock heating of laser-driven targets and the effect of that heating on target stability be measured. This Letter presents the first experimental demonstration of a correlation between higher shock temperatures produced early in the interaction and increased hydrodynamic stability.

Heating by shocks is dependent upon the shock strength causing the compression. The two cases examined in these experiments are meant to contrast two modes of compression. A rapid-rising square pulse produces a single strong shock that increases the isentrope of the compression, significantly heating the target. A slow-rising ramp pulse approximates a gentler (more isentropic) compression because the compression is achieved by a series of weaker shocks launched in progression as the drive pressure slowly increases. Since the increase in target adiabat (heating) is much less for the ramp pulse, it produces less ablative stabilization than the square pulse. In the absence of ablative stabilization, both cases should experience the same total RT growth for a given distance traveled, albeit at different times. These experiments demonstrate that the square pulse produces more shock heating and, as a result, produces results that behave very close to predictions by one-dimensional (1D) codes. In contrast, the results of the ramp-pulse experiments can be explained only if effects of the RT instability are considered.

Pulse shapes with different rise times were used to irradiate planar CH targets that had embedded Al layers, whose temperature was probed using time-resolved x-ray absorption spectroscopy. The $1s$-$2p$ Al absorption lines provided information about the ionization state of the Al, which, in turn, was used to infer both the shock-induced temperature and the heat-front propagation into the targets. The experiments indicate that steeply rising drive pulses produce shocks that heat the embedded Al layer to ~25 eV, while the slowly rising pulses produce shock heating below ~15 eV—our detection threshold. Targets driven by the rapidly rising pulses exhibit behavior that is readily predicted by 1D hydrodynamic simulations. It has been demonstrated in laser-driven-target experiments that the RT instability is seeded by laser imprinting [8] and causes mixing of the shell material. The result is a deviation from 1D behavior [9,10]. In the subject experiments, targets driven by slowly rising pulses exhibit that deviation and can be simulated if the mixing effects of the RT instability are included. These experiments show that the effect of this mix is diminished for the rapid-rise pulses because increased shock heating produces higher ablative stabilization.

In these experiments, 20-μm-thick CH targets were irradiated by six UV OMEGA [11] beams having 0.2-THz smoothing by spectral dispersion (SSD) [12]. A 0.5-μm-thick layer of Al was embedded at either 5 or 10 μm below the irradiated surface. The laser pulses were either (i) a steeply rising (~200-ps rise time), nearly square shaped pulse with 1 ns duration and on-target intensity of $\sim 4 \times 10^{14}$ W/cm^2 or (ii) a "ramp" pulse that rose linearly to 3×10^{14} W/cm^2 in 3 ns. One-dimensional calculations indicate that these pulses produce shock pressures of ~40 and ~15 Mb, respectively. The targets were probed with x rays from a microdot of Sm that were dispersed by a streaked x-ray spectrometer.

Figure 1(a) shows the time-resolved absorption spectrum from a 20-μm-thick CH target (with the Al layer 10 μm deep) irradiated with the square pulse. Along the

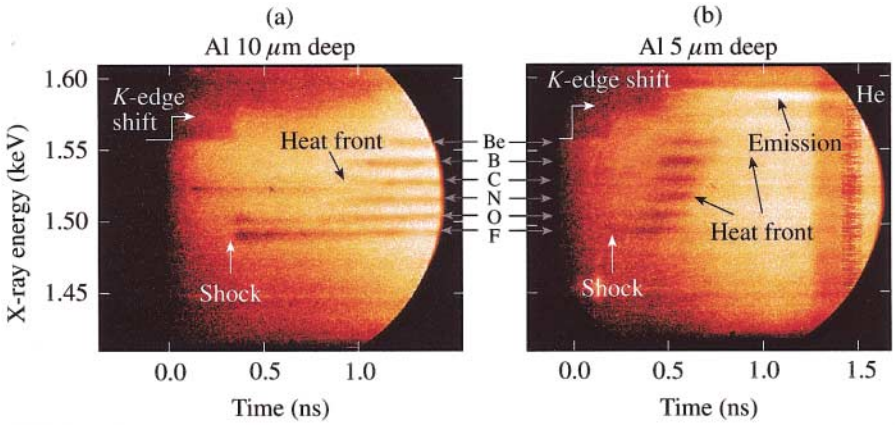

FIG. 1 (color). (a) Time-resolved absorption spectrum (dark horizontal bands) from an Al layer embedded 10 μm deep in a 20-μm-CH target irradiated by a square pulse. The F- and O-like absorption lines appear at ~320 ps due to shock heating. [Thin line starting at 100 ps and 1.525 keV is an instrument artifact.] Later (~800 ps) higher ionization states occur when the heat front reaches the Al. (b) Absorption spectrum with the Al layer 5 μm deep. The F- and O-like absorption lines appear at ~210 ps, and the heat front arrives at ~400 ps. He-like Al emission is observed when the heat front reaches the Al.

spectral direction, the $1s$-$2p$ absorption lines (dark bands) due to ionization states from F-like Al to Li-like Al are identified. The detailed structure of these transition arrays is not resolved, but their mean energies and widths are consistent with predictions [13] and other observations [14]. The data in Fig. 1(a) indicate that both F-like and O-like lines appear at ~320 ps, and then later, at ~800 ps, higher ionization states appear in progression.

Time is referenced to the start of the drive pulse that is preceded 300 ps by the backlighter. This allows observation of the K-shell absorption edge (at ~1.56 keV) in cold Al. At approximately the same time that the F-like and O-like lines appear, the K edge shifts to higher energy. This results primarily from the change in ionization of the Al ions. Later, as higher ionization states (N-like and above) appear, the K edge shifts to still higher energy.

The abrupt onset of the F-like and O-like absorption lines is caused by shock heating of the Al layer; the higher ionization states, which appear later, result from heating by the laser-driven heat front. These dynamics are confirmed by data from a target with the Al layer closer to the surface. Figure 1(b) is the spectrum from an experiment with the Al layer 5 μm deep. Here, the onset of the F-like and O-like Al absorption lines is not clear, but one can readily see the abrupt change in the K-edge energy occurring at ~210 ps, consistent with the shock speed inferred from Fig. 1(a). For the 5 μm CH, the heat front also arrives earlier (~400 ps), but, in this case, the heating is sufficient to not only create absorption in higher ionization states but also produce He-like emission. The He-like emission occurs because the heat front has penetrated the 5 μm CH and ablated the Al. The absorption lines are short lived because the temperature rises sufficiently to reduce the population in the lower tail of the charge-state distribution.

The dependence of shock heating on the temporal profile of the drive was measured by driving similar targets with the ramp pulse. Figure 2 shows an extended temporal record of absorption spectra from a target having the Al layer 5 μm deep and irradiated by the ramp pulse. The backlighter produces bright, broadband emission that ceases at ~2 ns. Coincidentally, at that time He-like Al emission begins, which indicates that portions of the Al are heated to over 500 eV. Preceding this emission, no Al absorption lines (1.48 to 1.56 keV) are observed. Similar experiments on targets with the Al 10 μm deep also showed no absorption lines on these shots; the He-like emission occurred ~400 ps later than shown in Fig. 2. These results are significant for two reasons: (1) They indicate the absence of significant shock heating before emission begins. (Note, however, that the K edge at 1.56 keV becomes quite diffuse after 1 ns, suggesting some low-level shock heating [15].) (2) The lack of absorption lines preceding the He-like emission suggests that Al is instantaneously heated from <15 to >500 eV, contrary to expected behavior. Heat

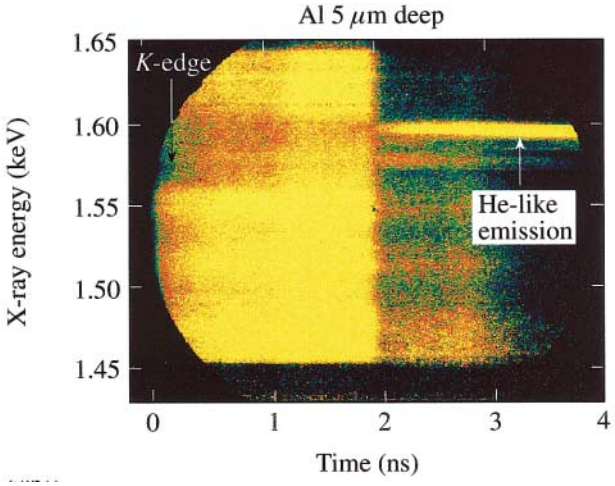

FIG. 2 (color). Absorption spectra from a target with the Al layer 5 μm deep and irradiated by a ramp pulse. No Al absorption lines are observed preceding the Al He-like emission lines that begin at ~1.9 ns.

fronts in both directly driven [16] and indirectly driven targets [14] normally exhibit a succession of Al absorption lines that appear before the emission lines, as in Fig. 1(b).

In summary, the slowly rising ramp pulse produces less shock heating (no absorption lines) than the square pulse, and targets driven by the ramp pulse show no Al absorption lines even in the presence of He-like emission. The latter observation will be attributed to effects of the RT instability, while the former demonstrate the effect of shock heating on target stability.

The relative populations of Al charge states and the resulting absorption spectra (for steady-state conditions at various temperatures) were calculated [17]. This allowed the Al temperature to be inferred as a function of time. Figure 3 shows the Al temperature measured (points) and predicted (curves) by 1D simulations (LILAC [18]). Figure 3(a) compares calculations and measurements for square-pulse irradiation of targets with the Al layer 5 μm deep (solid line and circles) and 10 μm deep (dashed line and triangles). Both the shock heating of the Al to $\sim$25 eV and the heat-front penetration ($> \sim 40$ eV) are correctly predicted by the 1D simulations, indicating stable target behavior. The minor discrepancy in timing of the heat-front arrival is likely the results of 2D effects (see below). The lower limit for this measurement technique is the onset of F-like absorption lines that occurs at about 15 eV. The error bars indicate a $\pm$100-ps timing uncertainty in the camera and a $\pm$10-eV precision of the temperature determination.

Similar temperature profiles for the ramp pulse are shown in Fig. 3(b) [5 μm deep (solid/square); 10 μm deep (dashed/triangle)]. Since there were no absorption lines in the data, only the onset times for Al emission (defined as 500 eV) are shown. The predicted temperatures are below the $\sim$15-eV experimental detection threshold until about 1.7 ns when the heat front arrives at the Al, which reaches $\sim$500 eV at 1.9 ns for the 5-μm case. The 10-μm case is not predicted to be heated above $\sim$40 eV, yet the experiment reaches 500 eV at $\sim$2.3 ns. The rate of rise predicted (by a 1D code) for the ramp pulse is similar to that for the square pulse [Fig. 3(a)], indicating that the lack of absorption lines is not due to a steep temperature rise.

To explain the observation that the heat front reaches the 10-μm-deep Al layer and the He-like emission occurs with no preceding Al absorption lines, the existence of a mixing region is postulated. The emission lines could result from Al that is prematurely mixed into the ablation region [10]. Using the model discussed in Ref. [19], the thickness of the mix layer was calculated and then added to the 1D simulations. The mix layer is produced by the RT instability that amplifies imprinted perturbations [11] producing considerable two-dimensional effects. The model uses the measured spectrum of irradiation nonuniformities to calculate the imprinted perturbations and then calculates their growth [20] and saturation [21]. Figure 4 shows the calculated and measured location of the ablation surface in units of the uncompressed CH thickness for the square and ramp pulses. (Once ablated, material must traverse the conduction zone before it is heated in the corona.) The dark lines are the predictions of 1D calculations, and the shaded regions are the calculated mix layers centered on those predictions. Figure 4 shows that the square-pulse data should not be significantly affected by the RT instability and should therefore be reasonably predicted by 1D simulations. In contrast, the ramp pulse has a mix layer that affects the apparent penetration at both 5- and 10-μm depths in the original target. The temporal offset ($\sim$250 ps) between the data and simulations corresponds to the time for the Al to travel from the ablation surface to the 500-eV isotherm [22]. This explains both the unexpected emission from the Al [10-μm result in Fig. 3(b)] and the lack of preceding absorption lines for the 5- and 10-μm cases. Specifically, the RT spikes can "leach" Al from the embedded layer out into the corona (where it emits), whereas the Al in the bubbles has not been heated significantly and therefore has no absorption signature. The relative size of the bubbles and spikes is such that the bubbles dominate the radiography (no absorption), while the bright (but smaller-sized) spikes are detected in emission but not resolved in absorption.

Simulations indicate that the square and ramp pulses both drive these targets $\sim$50 μm by the time the heat front has penetrated 5 μm of CH. In a laser-ablation-driven target, the linear-phase RT growth of perturbations is given

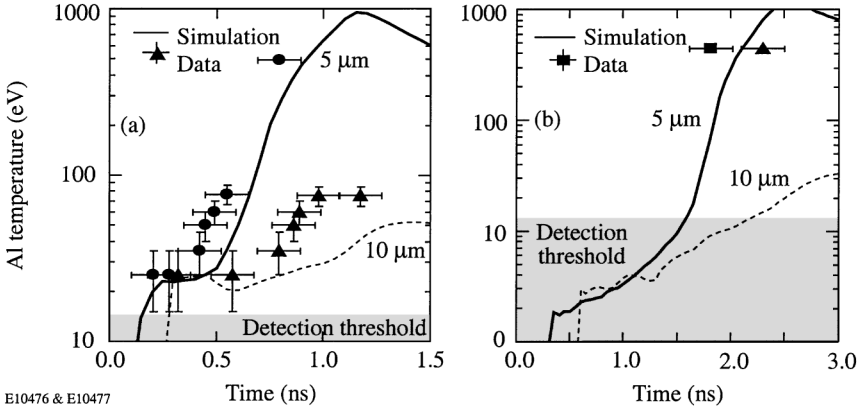

FIG. 3. Comparison of the temperatures of the embedded Al layer as predicted by the 1D code LILAC (curves) for various experiments and experimental data (points). (a) Square pulse driving the 5-μm case (solid line/circles) and the 10-μm case (dashed line/triangles). (b) Ramp pulse driving the 5-μm case (solid line/square) and the 10-μm case (dashed line/triangle). Ramp-pulse data were present only for emission lines.

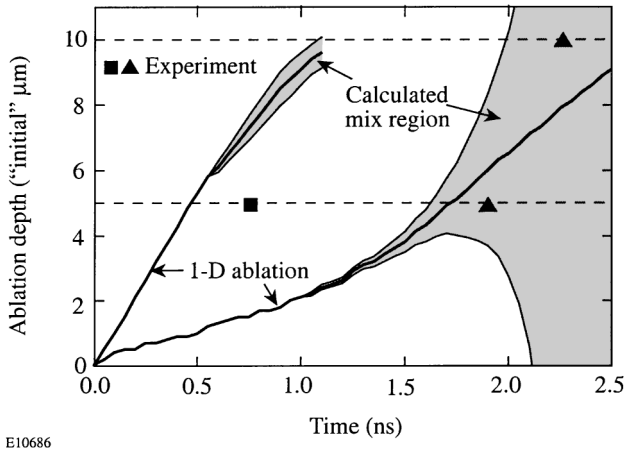

FIG. 4. The ablation depths in uncompressed CH thickness. The heavy lines are the 1D simulations, and the gray region is the calculated thickness of RT mixing. The measured penetration times are plotted at the embedded layer depths for the experiments.

as $A(t) = A_0 \exp(\int \gamma\, dt)$, where A_0 is an "initial" perturbation and γ is the growth rate given by $\gamma = \alpha\sqrt{kg} - \beta k V_a$ [4–6], where k is the perturbation wave number, g is the acceleration, and α and β are constants dependent upon laser and target parameters [6]. The total growth experienced by a target is therefore proportional to $\int \sqrt{g}\, dt$, which is proportional to its displacement. The target trajectory (i.e., acceleration history) represents a zeroth-order measure of the coupling of the laser to the target. The accuracy of the hydrocode LILAC to predict target acceleration has been verified extensively [23]. Experiments have demonstrated that, with SSD applied to the drive laser, slow-rising pulses (ramps) produce the same level of imprinting as do fast-rising pulses (squares) [8]. This is a result of the balance between optical smoothing and plasma smoothing for the two pulses. Nevertheless, these simulations still include a full treatment of imprinting that is consistent with our model [24] and experiments [8]. Thus, both pulses produce the same level of seed (A_0) for the RT instability. Then, in the absence of any stabilizing mechanisms, both pulses should experience similar RT instability (seed and growth). Instead, targets irradiated by these two pulse shapes behave differently because the square pulse produces a shock that heats the target to ~25 eV, causing it to decompress, thereby increasing the ablation velocity (V_a). This lowers the RT growth rate compared to that of the ramp pulse, which experiences less shock heating (<15 eV) and therefore has little ablative stabilization. The simulations (which correctly model the observed shock temperatures) confirm that the square pulse produces ablation velocities that are as much as 5 times larger than those for the ramp pulse.

It has been shown that, for the square-pulse drive, 1D simulations accurately predict the observed shock heating (~25 eV) produced by a ~40-Mb shock and the heat-front penetration depth. In contrast, the ramp pulses produce ~15-Mb shocks that do not appreciably heat the target (<15 eV). The targets exhibit apparent anomalous heat-front penetration that results from two-dimensional effects caused by the RT instability [19]. Simulations of these experiments indicate that the shock heating produced by rapidly rising pulses causes the target to decompress, creating higher ablation velocities that reduce the RT growth rates. In contrast, the slowly rising pulse causes considerably less shock heating, producing less ablative stabilization, and therefore experiences significant effects due to the RT instability. This confirms the expected effect of shock heating and ablative stabilization on the stability of directly driven ICF targets.

This work was supported by the U.S. Department of Energy Office of Inertial Confinement Fusion under Cooperative Agreement No. DE-FC03-92SF19460, the University of Rochester, and the New York State Energy Research and Development Authority. The support of DOE does not constitute an endorsement by DOE of the views expressed in this article.

[1] J. D. Lindl, Phys. Plasmas **2**, 3933 (1995).
[2] S. E. Bodner *et al.,* Phys. Plasmas **5**, 1901 (1998).
[3] J. D. Kilkenny *et al.,* Phys. Plasmas **1**, 1379 (1994).
[4] S. E. Bodner, Phys. Rev. Lett. **33**, 761 (1974).
[5] H. Takabe, L. Montierth, and R. L. Morse, Phys. Fluids **26**, 2299 (1983).
[6] R. Betti *et al.,* Phys. Plasmas **3**, 2122 (1996).
[7] E. M. Campbell, W. J. Hogan, and D. H. Crandall, in *Inertial Fusion Sciences and Applications 99,* edited by C. Labaune, W. J. Hogan, and K. A. Tanaka (Elsevier, Paris, 2000), p. 9.
[8] T. R. Boehly *et al.,* Phys. Plasmas **8**, 2331 (2001).
[9] D. D. Meyerhofer *et al.,* Phys. Plasmas **8**, 2251 (2001).
[10] D. K. Bradley, J. A. Delettrez, and C. P. Verdon, Phys. Rev. Lett. **68**, 2774 (1992).
[11] T. R. Boehly *et al.,* Opt. Commun. **133**, 495 (1997).
[12] S. Skupsky and R. S. Craxton, Phys. Plasmas **6**, 2157 (1999).
[13] C. Chenais-Popovics *et al.,* Phys. Rev. A **42**, 4788 (1990).
[14] T. S. Perry *et al.,* J. Quant. Spectrosc. Radiat. Transfer **51**, 273 (1994).
[15] T. A. Hall *et al.,* Europhys. Lett. **41**, 495 (1998).
[16] D. Hoarty *et al.,* Phys. Rev. Lett. **82**, 3070 (1999).
[17] D. Hoarty *et al.,* Phys. Rev. Lett. **78**, 3322 (1997).
[18] M. C. Richardson *et al.,* in *Laser Interaction and Related Plasma Phenomena,* edited by H. Hora and G. H. Miley (Plenum Publishing, New York, 1986), Vol. 7, p. 421.
[19] J. Delettrez, D. K. Bradley, and C. P. Verdon, Phys. Plasmas **1**, 2342 (1994).
[20] R. Betti *et al.,* Phys. Plasmas **5**, 1446 (1998).
[21] S. W. Haan, Phys. Rev. A **39**, 5812 (1989).
[22] J. A. Delettrez *et al.,* Bull. Am. Phys. Soc. **45**, 224 (2000).
[23] R. L. McCrory *et al.,* in *Laser Interaction with Matter,* edited by G. Velarde, E. Minguez, and J. Perlado (World Scientific, Singapore, 1989), p. 73.
[24] V. N. Goncharov *et al.,* Phys. Plasmas **7**, 2062 (2000).